

# 2

## *Theory and Experiment: The Scientific Motivation*

**P**roton-induced pion production, in “elementary”  $pN \rightarrow NN\pi$  processes and in light nuclei, has been an intensely active area of study in intermediate energy nuclear physics over recent years. Pions, being the least massive mesons, are fundamental to the most successful, modern descriptions [Ma87] of the nucleon-nucleon interaction. A full understanding of proton-induced pion production is an important component of a complete description of the nuclear strong force. This chapter describes the theoretical and experimental motivations for the study of  $A(p, \pi)A+1$  and  $A(p, \pi\pi)A+1$  in general and for the CE-06 experiment in particular.

### **2.1 Theoretical Concepts, Models, and Predictions**

#### **2.1.1 Elementary Pion Production Processes: $NN \rightarrow NN\pi$**

Pions are specific examples of *mesons*: that collection of strongly interacting particles which are also bosons, and are comprised solely of quark-antiquark pairs. As such, any number of pions can be created or absorbed in collisions between two nucleons. Table 2.1 shows the seven possible  $NN \rightarrow NN\pi$  reactions for which at least one of the nucleons in the incident channel is a proton. For protons with energies  $E_p \approx 300$  MeV, the probe size is  $\lambda_p \approx 1.5$  fm, so that for  $(p, \pi)$  reactions, even in heavy nuclei, the channels listed would be expected [Ma79] to play an important role in the production process.<sup>[1]</sup> Since the  $Q$ -value

---

<sup>[1]</sup> A truly complete calculation of  $A(p, \pi)A+1$  would, in fact, predict the elementary reaction cross-

for these inelastic N-N reactions is  $Q \approx -m_\pi$ , the threshold proton kinetic energies are  $E_{p,\text{thr}} \approx 2m_\pi \approx 280$  MeV.

pN $\rightarrow$ NN $\pi$ Reaction	Isospin Decomposition
$p + p \rightarrow d + \pi^+$	$\sigma_{10}(\text{d})$
$p + p \rightarrow p + n + \pi^+$	$\sigma_{10}(\text{np}) + \sigma_{11}$
$p + n \rightarrow n + n + \pi^+$	$\frac{1}{2}(\sigma_{01} + \sigma_{11})$
$p + n \rightarrow d + \pi^0$	$\frac{1}{2}\sigma_{10}(\text{d})$
$p + p \rightarrow p + p + \pi^0$	$\sigma_{11}$
$p + n \rightarrow p + n + \pi^0$	$\frac{1}{2}(\sigma_{10}(\text{np}) + \sigma_{01})$
$p + n \rightarrow p + p + \pi^-$	$\frac{1}{2}(\sigma_{01} + \sigma_{11})$

*Table 2.1* The elementary pN  $\rightarrow$  NN $\pi$  reactions and corresponding total cross-section isospin decompositions, labelled by  $\sigma_{T_i T_f}$ , where  $T_i$  and  $T_f$  are the isospin states of the initial and final nucleon pairs, respectively. The factors of 1/2 appear since the incident p + n state can be both  $T = 0$  or  $T = 1$ .

To the extent that electromagnetic effects can be ignored (early measurements [Wi71] of  $pn \rightarrow d\pi^0$ , for example, showed that isospin-violating contributions are at the 1% level), the total reaction cross-sections can be decomposed in terms of the isospin of the initial and final nucleon pairs, as shown in Table 2.1. With this decomposition, several interesting points can be made. Since the pion is a  $T = 1$  state, there can be no contribution from the isospin singlet-singlet channel  $\sigma_{00}$  for the  $pn \rightarrow d\pi^0$  and  $pn \rightarrow pn\pi^0$  reactions. For the latter, furthermore, there is no contribution from  $\sigma_{11}$ , since the appropriate Clebsch-Gordan coefficient,  $\langle T = 1, M = 0 | m_{\text{NN}} = 0, m_\pi = 0 \rangle$ , vanishes. These seven reactions can therefore be described by the four parameters  $\sigma_{10}(\text{d})$ ,  $\sigma_{10}(\text{np})$ ,  $\sigma_{11}$ , and  $\sigma_{01}$ . Finally, the table shows that whereas  $\pi^+$  and  $\pi^0$  production are equally represented by three channels,  $\pi^-$  production is possible only via  $pn \rightarrow pp\pi^-$ .

Probably the simplest mechanism through which elementary pion production can occur at intermediate energies is via  $NN \rightarrow N\Delta \rightarrow NN\pi$ , where  $\Delta$  is the  $T = 3/2$ ,  $J = 3/2$  resonance with  $m_\Delta \approx 1232$  MeV. This mechanism has in fact long been known [Lm70] to dominate  $pp \rightarrow d\pi^+$ : a very strong, broad peak is evident in  $\sigma(E_p)$ , for  $\sqrt{s} \approx m_p + m_\Delta$ , where  $s$  is the square of the total four-momentum. More recently, non-phenomenological models of  $NN \rightarrow NN\pi$  [Du87] have confirmed the  $\Delta^{++}$  dominance in this reaction. For

---

sections of Table 2.1 in a few-nucleon simplification of the model.

such a process to occur, the initial isospin channel must be  $T = 1$  since  $T(N\Delta) \geq 1$ . The  $\sigma_{01}$  amplitude of Table 2.1 should therefore be small, and experimental data [Ma79] suggests that this is so. For proton energies in the 500 MeV range, in particular,  $\sigma_{10}(d) > \sigma_{10}(pn) > \sigma_{11} > \sigma_{01}$ , so that  $\sigma(pp \rightarrow d\pi^+)$  and  $\sigma(pn \rightarrow d\pi^0)$  ( $= \sigma(pp \rightarrow d\pi^+)/2$ ) are the dominating cross-sections.

Despite long-term efforts to model theoretically the excitation functions and angular distributions of these reactions<sup>[2]</sup>, problems in the calculations remain, especially near threshold [Bl90] where the  $\Delta$  resonance is not as important. For example, only the Ss, Sp, Ps, and Pp states (using the standard spectroscopic notation  $L_{NN}l_\pi$  for the exit channel partial waves) should contribute significantly for  $E_p \lesssim 400$  MeV. For the  $pp \rightarrow pp\pi^0$  reaction in particular, only the Ss state is important close to the reaction threshold. Nonetheless, not until recently [Le93] have theoretical predictions been successful in describing the total cross-section for this reaction.<sup>[3]</sup>

### 2.1.2 Single-Pion Production in Light Nuclei: $A(p, \pi)A+1$

Although the reactions listed in Table 2.1 can be expected to contribute significantly to pion production in nuclei, there are several new considerations involved in studies of  $(p, \pi^+)$  on more complex ( $A \geq 3$ ) systems:

- a) “sub-threshold” pion production (i.e., at proton energies below the threshold for elementary production) can occur, due in part to the Fermi motion of the nucleons in a bound nuclear state;
- b) multiple interactions, such as internal charge exchange ( $\pi^0 p \rightarrow \pi^- n$ ), or absorption on a nucleon pair ( $\pi^0 np \rightarrow np$ ) may take place (reducing exclusive  $(p, \pi)$  cross-sections for heavy nuclei compared to light systems);
- c) the Pauli principle and spin considerations can forbid or simplify some reaction processes: the population of a ground state nucleus, for example, may eliminate underlying contributions from some of the processes in Table 2.1;
- d) collective nuclear effects can be important: the nucleus may act as a whole in  $A(p, \pi)A+1$  processes.

Much theoretical work has been carried out [Fe81] since the early 1970’s to develop models of  $A(p, \pi)A+1$ , instigated (at least initially) by the motivations of Ch. 1. All

---

[2] Phenomenological models for  $NN \rightarrow NN\pi$  were first described [Ge54] in 1954.

[3] This is indicative, in fact, of the lack of knowledge concerning the very short-range part of the N-N interaction.

of these models incorporate some or all of the components diagrammed schematically in Fig. 2.1. Multi-nucleon effects are included through nuclear bound-state wave functions and initial and final state distortions. The wave functions directly incorporate the system's nuclear structure in the model; in fact, the use of  $A(p, \pi)A+1$  as a structure probe was a primary motivation in these studies. However, the complexities involved in understanding the reaction mechanism have turned the problem around. For example, more recent model calculations ([Be92], [Co82]) tend to incorporate tractable nuclear wave functions (or those which are well-defined in terms of the shell model) to achieve insight into the fundamental production processes.

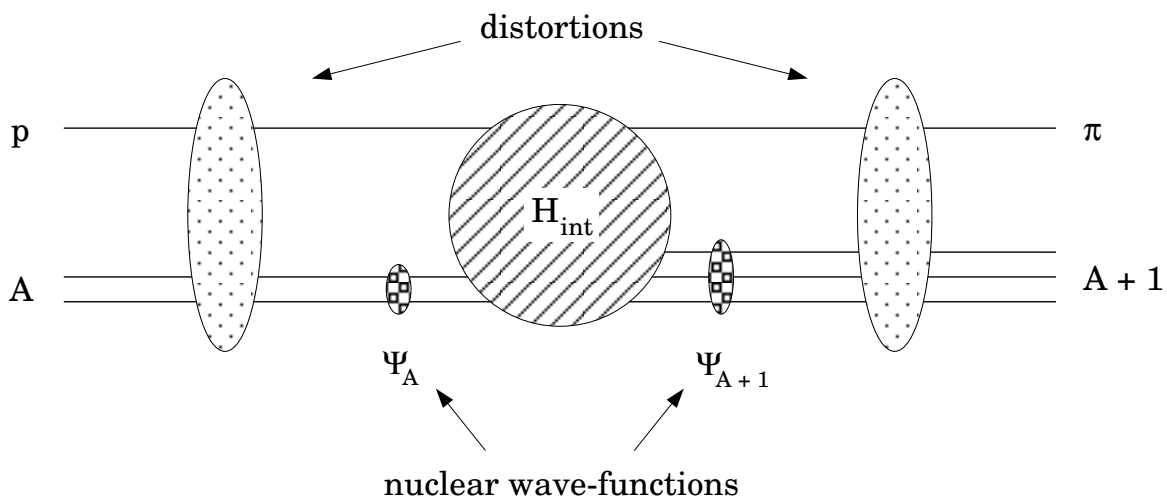


*Figure 2.1* The primary components involved in modern model calculations of  $A(p, \pi)A+1$ : a) proton-nucleus and pion-nucleus distortions; b) nuclear wave-functions; and c) the fundamental pion production process  $H_{int}$ .

The distortions included in the models account for the *average* effect of the initial and final nuclear states on the incident proton and outgoing pion, respectively. For the incident distortions, proton elastic scattering data (for the target nucleus in question) are typically used to generate phenomenological potentials of the proton-nucleus interaction. Similarly, the pion-nucleus distortions are usually incorporated by the calculation of optical-model parameters to describe pion-nucleus elastic scattering (for the final state nucleus in question). Both the proton and pion distortion potentials include Coulomb effects and, in fact, typically describe low-energy elastic scattering [Ks84]; however, more recent calculations [Be90] allow the inclusion of both resonant ( $\Delta$  formation) and non-resonant pion-nucleus scattering potentials.

Although the nuclear wave functions and distortions are an important component of

all current models, much of the modern interest in  $(p, \pi)$  reactions lies in determining the structure of the complex pion-production interaction labelled by  $H_{\text{int}}$  in Fig. 2.1. Models are conventionally classified according to whether  $H_{\text{int}}$  explicitly includes a single nucleon (the “one-nucleon mechanism” or ONM) or two nucleons (TNM).<sup>[4]</sup> Conceptually, the ONM and TNM models can be described as  $N \rightarrow N\pi$  and  $NN \rightarrow NN\pi$  processes, respectively, within the nuclear medium.

The  $N \rightarrow N\pi$  process is the simplest means by which a pion can be produced, although conservation of momentum and energy forbid the free  $N \rightarrow N\pi$  reaction (unlike the elementary  $NN \rightarrow NN\pi$  processes of Sec. 2.1.1). For a proton projectile, the ONM production processes are:  $p \rightarrow n\pi^+$ ,  $p \rightarrow p\pi^0$ , and  $p\pi^- \rightarrow n$ . These reactions are possible in the nuclear medium since spectator nucleons are available to provide the needed momentum conservation.

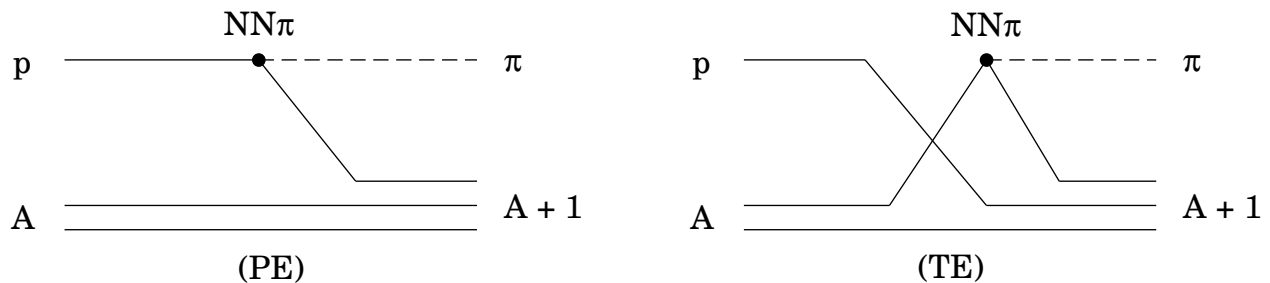


*Figure 2.2* Schematic diagrams underlying the  $H_{\text{int}}$  part of the ONM models. The two contributions are the projectile-emission (PE) diagram (left) and the target-emission (TE) diagram (right).

Figure 2.2 schematically shows the diagrams involved in the ONM calculations, which are often referred to as “pionic stripping” models from the similarity to  $(d, p)$  and  $(d, n)$  reactions. The ONM is further categorized by the left and right diagrams in the figure, corresponding respectively to projectile emission (PE) and target emission (TE) of the pion. Most current calculations (e.g., [Al88]) that involve the ONM include only the PE diagram, although some authors [Ks84] have argued that the TE diagram tends to cancel the PE contribution. Since the TE diagrams need to be summed over all target nucleons, however, it seems likely [Al88] that the TE contribution in itself is negligible.

In the simplest ONM scenario, such as a plane-wave Born approximation (PWBA), all of the (large) momentum transfer occurs via the single captured nucleon, so that the

---

<sup>[4]</sup> The ONM and TNM models are both multi-nucleon calculations, however, due to the inclusion of distortions and nuclear wave functions.

process directly samples the high-momentum components of the (single-particle) bound-state wave function. Since the momentum transfer in  $(p, \pi)$  reactions is typically much larger than the average Fermi momentum for a light nucleus, the PWBA picture tends to greatly underestimate [Fe81] the measured cross-sections. The inclusion of distortions in a more sophisticated calculation, however, removes this problem by allowing a further means of momentum sharing. Full, relativistic ONM treatments [Co82], in fact, reproduce differential cross-sections for  $(p, \pi^+)$  reactions leading to doubly-magic nuclei (in both strength and shape) with reasonable success. All ONM calculations to date are, however, quite sensitive<sup>[5]</sup> to the number (e.g., pion, proton, or both) and form (computational method or approximation) of the distortions used.

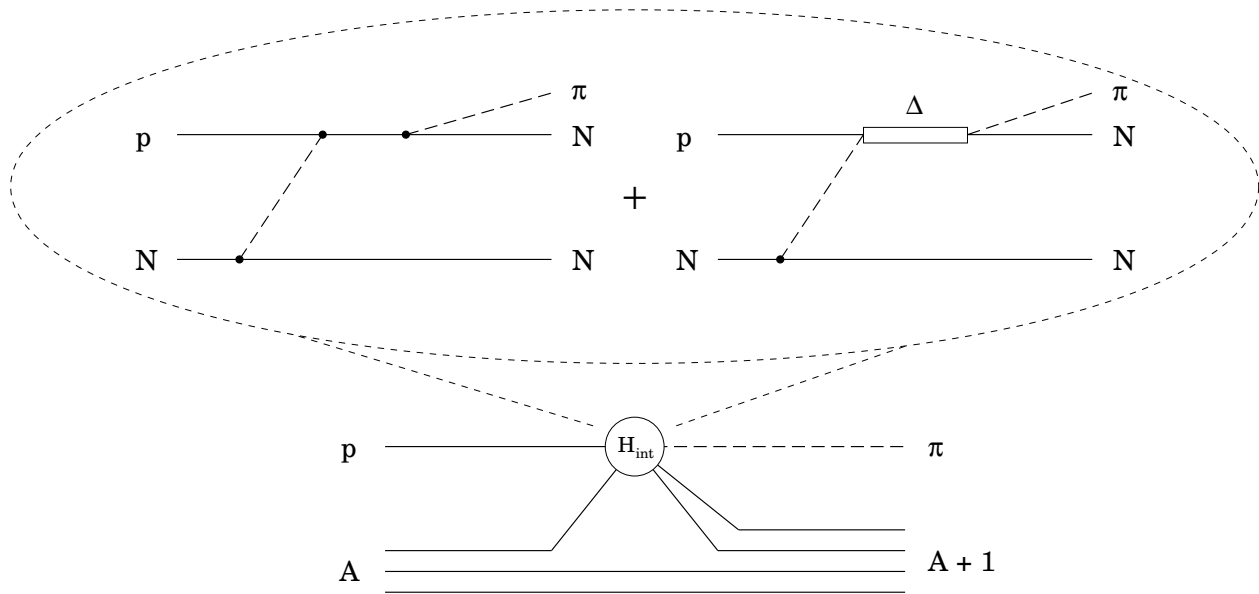


*Figure 2.3* Diagrams involved in the TNM calculation of the fundamental production process  $H_{\text{int}}$ . Only the “post-emission”, TE diagrams for resonant and non-resonant pion production are shown; in general, the corresponding PE diagrams and “pre-emission” contributions (where the outgoing pion is emitted before the virtual pion is absorbed) must also be included.

Figure 2.3 shows the diagrams involved in the TNM calculations, the next level of complexity in terms of  $H_{\text{int}}$ . This model can address specific deficiencies of the ONM calculations:  $\pi^-$  production (not allowed via PE ONM diagrams) can occur through the last process in Table 2.1; two-particle, one-hole (2p-1h) states in the final nucleus can be

<sup>[5]</sup> The resulting cross-sections may easily vary [Co82] by an order of magnitude or more for different types of distortions.

directly populated (the ONM can directly “reach” only single-particle states); and, the TNM does not rely as heavily on distortions for the needed momentum sharing, since the second nucleon is available to absorb some of the momentum transfer.

Another important aspect of the TNM is the capability for direct inclusion of the  $\Delta$  resonance, the excitation of which can actually simplify [Ks84] the TNM calculations. For  $(p, \pi^+)$  reactions with  $E_p \gtrsim 200$  MeV, in particular, the non-resonant diagrams of Fig. 2.3 are negligible [Iq85] in comparison to the resonant contributions. As discussed in Sec. 2.1.1, the  $\Delta$  resonance dominates elementary  $NN \rightarrow NN\pi$  processes at intermediate energies, hence the large contribution of resonant TNM diagrams to  $A(p, \pi)A+1$  is not unexpected.

The flexibility associated with TNM models does, however, imply considerable complexity in practical, microscopic calculations. For example, both PE and TE diagrams can contribute to the TNM, and the intermediate virtual boson can not only be a pion but also a (vector-isovector)  $\rho$  meson, even at near-threshold energies ( $E_p \approx 200$  MeV). Nonetheless, an extensive, microscopic description (the “ABCD” model) has recently been developed ([Al88], [Al89], [Be90]) which incorporates both ONM and resonant TNM diagrams. Although these calculations were primarily concerned with  ${}^3\text{He}(p, \pi^+){}^4\text{He}$ , several generally applicable conclusions can be drawn from this work. First, the ONM and TNM diagrams can, in general, both contribute significantly (and interfere) for a given reaction. In this way, it is not appropriate to state whether the ONM or the TNM is the “correct” production process; rather, the dominance (if any) of a particular mechanism over another for the particular reaction, proton energy, and final-state nucleus should be considered.

Second, the best results are often achieved when the nuclear states involved have well-defined shell model configurations. The application of the ABCD model to 2p-1h states [Be92] has shown considerable sensitivity to configuration mixing, as have other models [Co82] in calculations for (expected) single-particle states in carbon. Today, these sensitivities play a dual role as the *raison d’être* for  $(p, \pi)$  studies (for example, as a probe ([Ja85], [Vi82]) of high-spin excitations in nuclei) and as a complication in determining the fundamental production mechanism.

Finally, current calculations remain sensitive to initial and final state distortions. Although TNM calculations tend to demonstrate a weaker dependence [Iq85] on distortions than ONM models, higher-order TNM effects which are as yet not possible to include microscopically are not necessarily negligible [Di82]. A modern goal for these calculations

is the shifting of the sensitivity from distortion potentials to details of the pion production mechanism.

In summary, much progress has been made in the last two decades toward the development of fully microscopic models of pion production in nuclei. Although the most complete calculations are still sensitive to various “external” inputs such as nuclear wave functions or pion distortions, it is reasonable to hope that comparison between these models and (as yet non-existent) quark/gluon models will shed light on the form of the nuclear strong force. Through extensive comparison with  $(p, \pi)$  data (the primary test, of course, of  $A(p, \pi)A+1$  models), questions of the differences between the free and bound N-N interaction may well be answered.

### 2.1.3 Double-Pion Production in Light Nuclei: $A(p, \pi\pi)A+1$

For proton energies greater than  $E_p \approx 600$  MeV, the production of *two* pions in free NN collisions becomes kinematically feasible. The possible  $pN \rightarrow NN\pi\pi$  reactions are listed in Table 2.2, along with the corresponding reactions for proton bombardment on  $^{12}\text{C}$  leading to strongly-bound final-state nuclei. Relatively little theoretical work has been applied to understanding the elementary processes, compared to their single-pion counterparts in Table 2.1. This is at least partly due to the difficulty in obtaining exclusive cross-section data for these reactions out of the single-pion background.

$pN \rightarrow NN\pi\pi$ Reaction	$^{12}\text{C}(p, \pi\pi)$ Reaction
$p + p \rightarrow n + n + \pi^+ \pi^+$	$p + ^{12}\text{C} \rightarrow ^{13}\text{B} + \pi^+ \pi^+$
$p + p \rightarrow p + n + \pi^+ \pi^0$ $p + n \rightarrow n + n + \pi^+ \pi^0$	$p + ^{12}\text{C} \rightarrow ^{13}\text{C} + \pi^+ \pi^0$
$p + p \rightarrow p + p + \pi^0 \pi^0$ $p + n \rightarrow p + n + \pi^0 \pi^0$	$p + ^{12}\text{C} \rightarrow ^{13}\text{N} + \pi^0 \pi^0$
$p + p \rightarrow p + p + \pi^+ \pi^-$ $p + n \rightarrow p + n + \pi^+ \pi^-$	$p + ^{12}\text{C} \rightarrow ^{13}\text{N} + \pi^+ \pi^-$
$p + p \rightarrow p + n + \pi^0 \pi^-$	$p + ^{12}\text{C} \rightarrow ^{13}\text{O} + \pi^0 \pi^-$

*Table 2.2* The elementary  $pN \rightarrow NN\pi\pi$  reactions and corresponding double-pion production reactions from  $^{12}\text{C}$ . Reactions leading to final-state pn pairs also have deuteron counterparts (not shown). The  $\pi^- \pi^-$  elementary reaction (also not shown) leads to the unbound nucleus  $^{13}\text{F}$ .

The charge-exchange reactions  $(\pi^\pm, \pi^\mp)$  and  $(\pi, \pi\pi)$  processes, however, have been studied fairly extensively in recent years. Fig. 2.4 demonstrates the intimate connection

between the  $(\pi, \pi\pi)$  and  $(p, \pi\pi)$  reactions for two particular diagrams (called the “pion-pole” and “contact” terms). A complete model for  $(\pi, \pi\pi)$  must consider [Os85] many more diagrams: for example, those with intermediate  $\Delta$  states<sup>[6]</sup> or two and three pion vertices for each nucleon line. Although these diagrams can primarily contribute only as higher-order effects in single-pion production (and are “included” in the  $A(p, \pi)A+1$  models via distortions), the neglect of such non-linear terms in microscopic double-pion production calculations results [Os85] in significant underprediction of measured  $(\pi, \pi\pi)$  cross-sections.

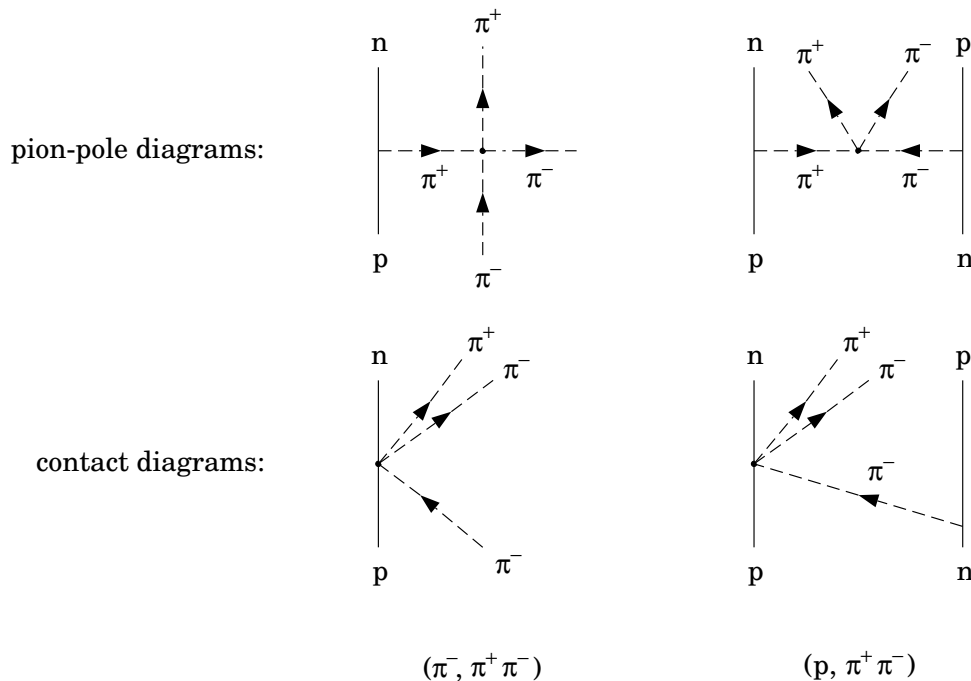


Figure 2.4 A comparison between the  $(\pi, \pi\pi)$  (left) and  $(p, \pi\pi)$  (right) reactions for two important contributing diagrams: the pion-pole (top) and contact (bottom) terms (as specific examples,  $(\pi^-, \pi^+ \pi^-)$  and  $(p, \pi^+ \pi^-)$  are shown). The diagrams are highly non-linear: three- and four-pion vertices are involved.

This complicated situation is greatly simplified ([Os85], [Jk90]) near the threshold of the  $(\pi, \pi\pi)$  reaction (and correspondingly for  $(p, \pi\pi)$ ). In particular, only four diagrams can contribute, two of which are the pion-pole and contact terms shown in Fig. 2.4 for both  $(\pi, \pi\pi)$  and  $(p, \pi\pi)$ . As third- and fourth-order pion diagrams, respectively, the contact and pion-pole diagram strengths directly reflect any possible underlying symmetry breaking in the chiral  $\pi N$  interaction. The contributions of the other two diagrams that do not vanish

<sup>[6]</sup> At  $E_p \approx 1.5$  GeV, for example,  $NN \rightarrow \Delta\Delta \rightarrow NN\pi\pi$  should [Lm70] be important.

near-threshold are not well-defined<sup>[7]</sup>. Nonetheless, the behavior of the very near-threshold cross-section for  $(\pi, \pi\pi)$  (and for  $(p, \pi\pi)$ ) as a function of incident pion (proton) energy is sensitive [Os85] to this symmetry breaking (if it exists). No data for  $(\pi, \pi\pi)$  as yet exists for  $E_\pi < 200$  MeV, and similarly for elementary  $(p, \pi\pi)$  with  $E_p \lesssim 700$  MeV [Dh83].

A related interest in these reactions is the possible formation of quasi-bound ( $\Gamma \approx 30$  MeV), multiple-pion states within the nuclear medium. These states could, for example, consist [Sk88] of  $(\pi\pi)_{J=0}^{T=0}$  pairs, analogous to electron Cooper pairs. Other authors [Ei80] suggest that double-pion production reactions would be sensitive to effects indicative of Bose condensed pion groups; however, the  $(\pi, \pi\pi)$  sensitivity to such “pre-cursor” phenomena has recently been questioned [Os86].

Although the similarity of  $(p, \pi\pi)$  and  $(\pi, \pi\pi)$  is evident from Fig. 2.4, one can infer from the discussion in Sec. 2.1.2 that proton-induced double-pion production in light nuclei will in general be more complicated than the elementary  $(\pi, \pi\pi)$  processes. Near threshold, however, it may at least be possible [Wa52] to distinguish the production mechanism from  $\pi\pi$  interaction effects. Furthermore, as with single-pion production, isospin constraints can simplify the picture somewhat.

For example, the contact term of Fig. 2.4 does not [Di89] contribute, near threshold, to the  $^{13}\text{B}$  reaction in Table 2.2, whereas both diagrams can contribute to the  $^{13}\text{C}$  reaction. Determination of the ratio  $\sigma(^{13}\text{B})/\sigma(^{13}\text{C})$  near threshold, therefore, directly measures the relative strengths of these two diagrams. Similarly to  $(p, \pi)$  studies, it is hoped that cross-section data for  $A(p, \pi\pi)A+1$ , perhaps near threshold, may reveal much about the NN interaction within the nucleus.

## 2.2 Experimental Motivations: Data, Anomalies, and Resonances

The theoretical motivations of Sec. 2.1 can hardly be considered to be independent of the experimental data for pion production in light systems. In this sense, the need for high-quality data as a basis of comparison for models of single- and double-pion production is an important experimental motivation ([Fe81], [Ma79]) for these studies. Rather than reviewing the complete body of existing pion-production data, however, this section considers specific, recent experimental developments in pion production which the CE-06 experiment hopes to address in particular.

---

[7] The strengths of these diagrams depend indirectly [Os85] on the characteristics of the  $\sigma$  “resonance” of Table 1.1.

### 2.2.1 Single-Pion Production

Cross-section data for several of the proton-induced, elementary pion production reactions in Table 2.1 have been available [Jo82] for more than a decade, and in particular for proton energies in the realm of the  $\Delta$  resonance ( $E_p \approx 600$  MeV). More recently, very near-threshold measurements ( $E_p \lesssim 320$  MeV) of  $pp \rightarrow pp\pi^0$  ([Me90], [Me92]),  $pp \rightarrow pn\pi^+$  [Ha93], and  $pp \rightarrow d\pi^+$  [He93] cross-sections have added significantly to the data base for  $NN \rightarrow NN\pi$  reactions.

The situation for  $(p, \pi^+)$  data in light nuclei is now, however, somewhat different: Due in part to the possibility of sub-threshold pion production, a fair amount of high-resolution  $(p, \pi^+)$  data exists ([Gr83], [So81], [Hd80]) near threshold ( $E_p \lesssim 200$  MeV), but not in the realm of the  $\Delta$  ( $200 \text{ MeV} \lesssim E_p \lesssim 400$  MeV). This lack of data is the case in particular for positive-pion production on carbon via  $^{12}\text{C}(p, \pi^+)^{13}\text{C}_{\text{g.s.}}$  (see Fig. 2.5), for which differential cross-sections have been measured at only three proton energies greater than  $E_p = 250$  MeV.

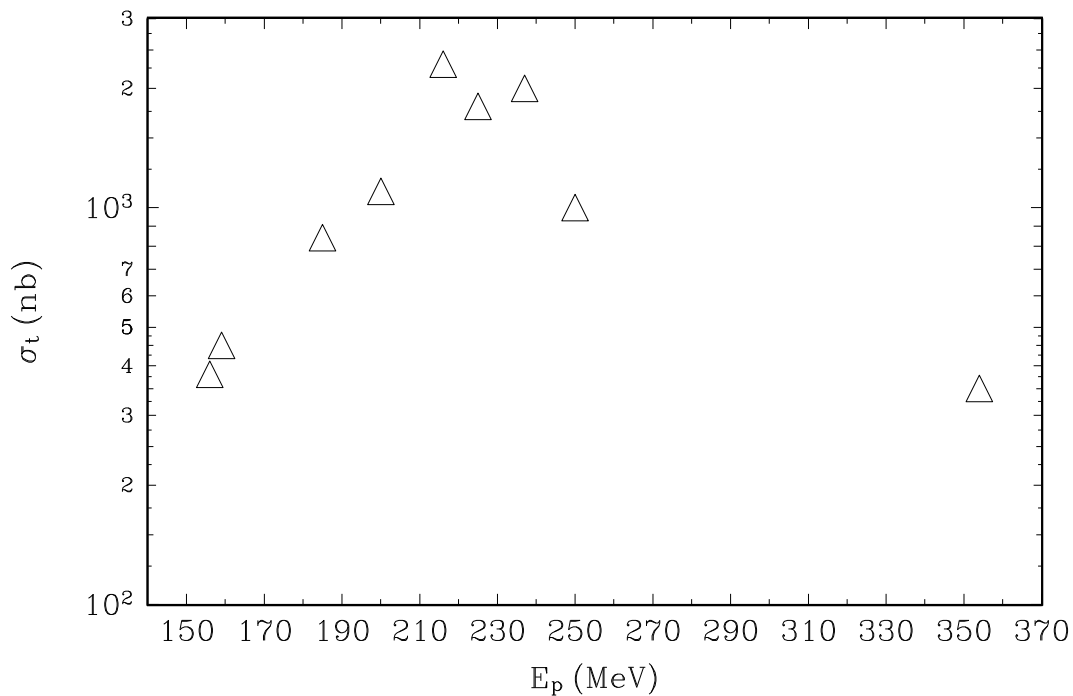


Figure 2.5 Total cross-section data for  $^{12}\text{C}(p, \pi^+)^{13}\text{C}_{\text{g.s.}}$  as a function of the incident proton energy. The data are from a variety of sources ([Hu87] and references therein).

The target  $^{12}\text{C}$  has received more attention in *near-threshold* pion production studies than other, light ( $A \lesssim 20$ ) nuclei for several reasons. Experimentally,  $^{12}\text{C}$  targets are

advantageous in that pure samples are readily available and easily constructed [Lz92] into solid targets of varying thicknesses. Also,  $^{12}\text{C}$  is the lightest nucleus (other than  $^4\text{He}$ ) which is stable and spinless in its ground state, simplifying experimental and theoretical treatments. Finally, the nuclei in the  $A = 12 - 14$  mass region, including the  $(p, \pi)$  reaction products from  $^{12}\text{C}$  targets, have been studied [Ko89] fairly extensively in other, high-momentum transfer reactions. Consequently, the nuclear structure in this mass region has been reasonably well-determined ([Aj90], [Aj91]).

Measurements of cross-sections for  $^{12}\text{C}(p, \pi^+)^{13}\text{C}$  and  $^{12}\text{C}(p, \pi^-)^{13}\text{O}$  in the  $\Delta$  resonance region are needed to fully map out the energy dependence of the total cross-section, as has been suggested before [Lo84]. Although the dominant role of the  $\Delta(1232)$  baryon in  $A(p, \pi^+)A+1$  seems to be on firm ground [Be92], the shift of the maximum of the excitation function [Hu87] below the  $\Delta$  invariant mass is somewhat surprising. Furthermore, data for  $^{12}\text{C}(p, \pi^-)^{13}\text{O}$  cross-sections with  $205 \text{ MeV} < E_p < 600 \text{ MeV}$  are non-existent and necessary to elucidate the role of non-resonant contributions that are important [Be92] at lower energies, compared to  $(p, \pi^+)$ .

The above considerations for studying pion production from  $^{12}\text{C}$  in the resonance region also apply to  $^{12}\text{C}(p, \pi^0)^{13}\text{N}$ . Even compared to  $^{12}\text{C}(p, \pi^-)^{13}\text{O}$ , the neutral pion reaction has received little attention, and to date there are only two studies ([Pi93], [Ho92]). In part, this lack of data is due to the experimental difficulty in measuring exclusive cross-sections for reactions with a neutral particle in the exit channel. Furthermore, one could argue that no fundamentally different information is available from  $(p, \pi^0)$ : the isospin amplitudes for the contributing two-nucleon elementary processes (see Table 2.1) are the same for  $\pi^+$  and  $\pi^0$ . The reactions  $^{12}\text{C}(p, \pi^+)^{13}\text{C}_{\text{g.s.}}$  and  $^{12}\text{C}(p, \pi^0)^{13}\text{N}_{\text{g.s.}}$  are, in particular, closely related due to the simple isospin structure of the target ( $T = 0$ ) and final-state ( $T = 1/2$ ) nuclei. After Coulomb corrections, the total cross-sections for these reactions are related by a simple ratio of Clebsch-Gordan coefficients:

$$R = \frac{\sigma(\pi^+)}{\sigma(\pi^0)} = \left( \frac{\sqrt{\frac{2}{3}}}{\sqrt{\frac{1}{3}}} \right)^2 = 2. \quad (2.1)$$

Nonetheless, an apparent discrepancy in this simple picture has itself provided motivation for further study of the  $^{12}\text{C}(p, \pi^0)^{13}\text{N}$  process in the threshold region. Fig. 2.6 shows a comparison between the total cross-sections for  $^{12}\text{C}(p, \pi^+)^{13}\text{C}_{\text{g.s.}}$  and  $^{12}\text{C}(p, \pi^0)^{13}\text{N}_{\text{g.s.}}$ , for  $E_p \lesssim 200 \text{ MeV}$ . For proton energies of 154 MeV ( $\eta \approx 0.34$ ) and 186 MeV ( $\eta \approx 0.78$ ), the measured ratio of the cross-sections is in good agreement with Eq. (2.1). However, at

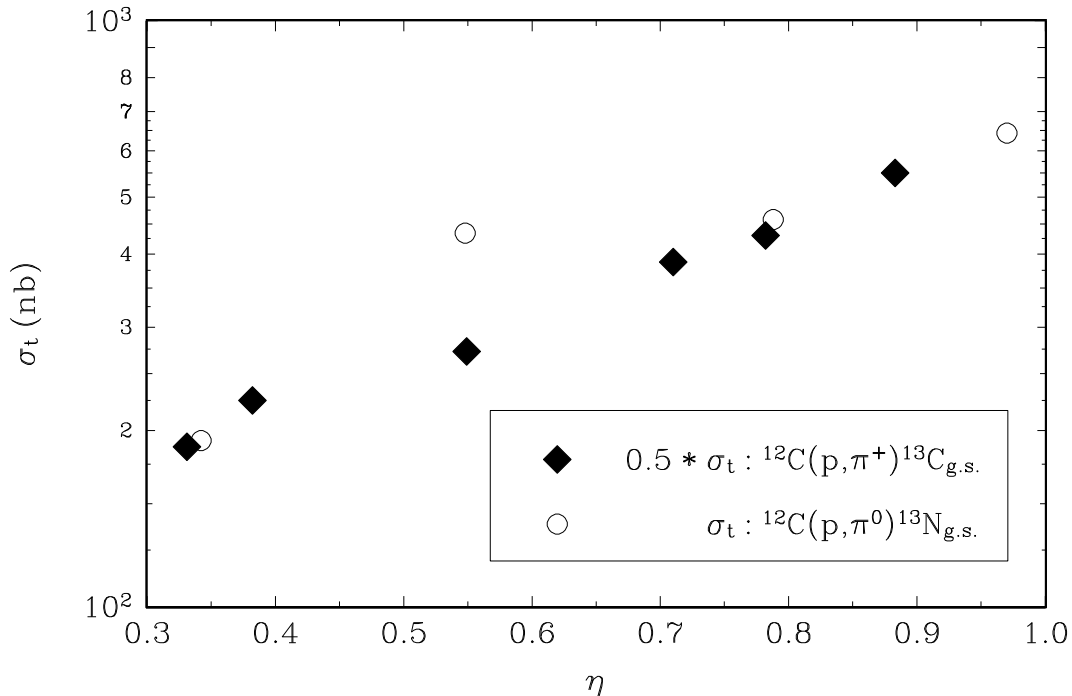


Figure 2.6 Comparison of the total cross-sections for  ${}^{12}\text{C}(p, \pi^+) {}^{13}\text{C}_{\text{g.s.}}$  and  ${}^{12}\text{C}(p, \pi^0) {}^{13}\text{N}_{\text{g.s.}}$  (adapted from [Ho92]), as a function of the center-of-mass reduced momentum  $\eta \equiv p_\pi/m_\pi c$ . The  $(p, \pi^+)$  cross-sections have been multiplied by a factor of 1/2 to account for Eq. (2.1).

$E_p = 166$  MeV ( $\eta \approx 0.55$ ), the ratio falls [Ho92] to  $R = 1.27 \pm .05$ . Pickar *et al.* [Pi93] have argued that Coulomb suppression of the low-energy  $\pi^+$  production can explain the 166 MeV discrepancy, although this analysis produces a similar but “opposite” anomaly ( $R = 2.8 \pm 0.4$ ) at 186 MeV, using the data of [Ho92] ( $\pi^0$ ) and [So81] ( $\pi^+$ ). In any case, there is clear need for confirmation of the anomaly (if it exists) via further measurements of  ${}^{12}\text{C}(p, \pi^0) {}^{13}\text{N}_{\text{g.s.}}$  for  $E_p < 200$  MeV.

## 2.2.2 Double-Pion Production

In contrast to the modern availability of  $A(p, \pi)A+1$  data, there are to date no exclusive studies of  $A(p, \pi\pi)A+1$  within 400 MeV of the threshold ( $E_p \approx 2m_\pi c^2$ ). Extrapolating from measured elementary  $NN \rightarrow NN\pi\pi$  cross-sections [Dh83] near  $E_p \approx 800$  MeV, the expected cross-sections would indeed be small: from approximately 1 to 100 nb. However, the corresponding  $\pi\pi$  production cross-sections may [Gn87] be significantly larger in nuclei. The only existing experimental study [Fn90] of  $A(p, \pi\pi)A+1$  ( $E_p = 800$  MeV) suggests that a cross-section measurement is feasible (i.e.,  $1 \text{ nb} \lesssim \sigma \lesssim 100 \text{ nb}$ ) even within 250 MeV of the threshold energy. Hence, the biggest *a priori* challenge in studies of  $A(p, \pi\pi)A+1$

may rest in the exclusivity of the measurement; as mentioned before, the background from single-pion production would be significant for intermediate energy protons.

Inclusive measurements of proton-induced pion production in nuclei *do* exist, however, and recent studies ([Kr82], [Ju84], [Ak92]) report an excessive production of low-energy pions (compared to that for high-energy pions) near  $E_p = 350$  MeV, which would seem to suggest an enhanced double-pion production. Although the possibility of the formation of  $(\pi\pi)$  bound states in nuclei has been suggested theoretically [Sk88] and experimentally [Ca93] in this energy range, the apparent width ( $\Gamma < 10$  MeV) of the resonance at  $E_p = 350$  MeV is much too narrow to be explained in this way. The enhancement may, however, be the result [Ku90] of the double-pion decay of a  $\Delta\Delta$  state in nuclear matter. Exclusive double-pion production data for  $E_p \approx 350$  MeV is clearly needed to confirm the existence of this structure.

### 2.2.3 CE-06: $^{12}\text{C}(\text{p}, \pi)$ and $^{12}\text{C}(\text{p}, \pi\pi)$ via the Recoil Method

Nearly all of the experimental studies of pion production in nuclei referred to in this section were accomplished via detection of the pion (or, one of the pions, in the case of the inclusive  $\pi\pi$  production experiments). Several very successful studies for  $E_p \lesssim 200$  MeV were completed using high-resolution spectrometers: notably, the Indiana QDDM and QQSP devices [Gr82]. However, the need for a large momentum bite (due to the large range in  $p_\pi$  possible even near threshold), large solid angle ( $(\text{p}, \pi)$  total cross-sections in light nuclei are typically less than 1 microbarn), and short pion flight paths (to reduce decay losses) greatly complicates the construction of the spectrometers. At higher energies ( $300 \text{ MeV} \lesssim E_p \lesssim 500 \text{ MeV}$ ), the emitted pions are magnetically very stiff ( $B\rho \approx 1$  T-m) and other detection methods [Fa86] must be employed. Furthermore, none of these techniques is applicable for studies of  $(\text{p}, \pi^0)$  or any exclusive measurements of systems with three-body final states.

The CE-06 experiment addresses these difficulties for the study of pion production from  $^{12}\text{C}$  by detection of the (heavy) recoil ion.<sup>[8]</sup> The method of recoil detection has several immediately apparent advantages for measurements of  $(\text{p}, \pi)$  in light nuclei. First, the determination of cross-sections for  $(\text{p}, \pi^+)$ ,  $(\text{p}, \pi^0)$ ,  $(\text{p}, \pi^-)$ , and  $(\text{p}, \pi\pi)$  can be accomplished simultaneously. Table 2.3 shows the possible recoil ions for the different charge states of the pion(s) emitted in  $^{12}\text{C} + \text{p} \rightarrow \pi(\pi) + \text{X}$ . Here, the detection of a mass-13 recoil ion uniquely specifies the reaction via conservation of baryon number. This ability to use

---

[8] The reaction nomenclature used in this work, however, always lists the recoil ion *last*.

$Q_{\pi(\pi)}$	$A = 13$ Ion	Possible Final States
+2	$^{13}\text{B}$	ground state only
+1	$^{13}\text{C}$	0.0, 3.09, 3.68, 3.85
+0	$^{13}\text{N}$	ground state only
-1	$^{13}\text{O}$	ground state only

*Table 2.3* Recoil ions obtained in pion production from proton bombardment of  $^{12}\text{C}$ , as specified by the total charge of the outgoing pion(s). Also given are the final-state nuclear excitation levels (MeV) that are accessible via the recoil method.

the same integrated beam, target, and detection system for several reaction measurements is clearly well-suited for studies of branching ratios into the different isospin channels.

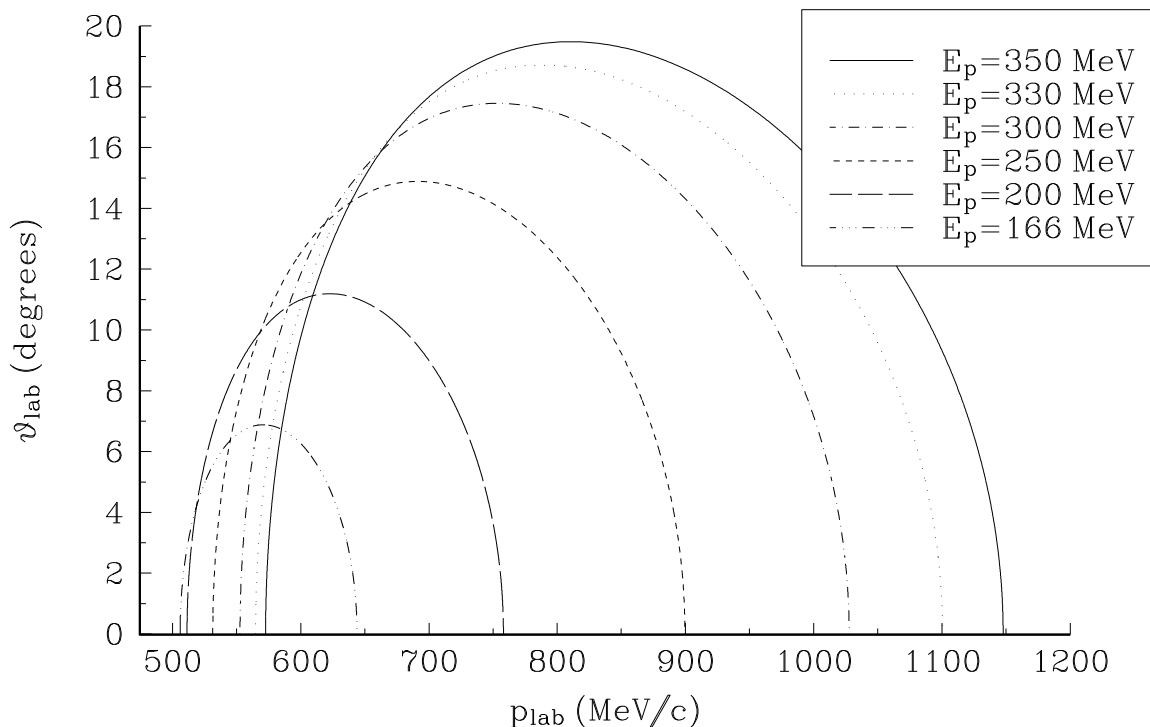


*Figure 2.7* Laboratory (target-at-rest) kinematics for  $^{12}\text{C}(p, \pi^+)^{13}\text{C}_{\text{g.s.}}$ , for several incident proton energies within 200 MeV of the reaction threshold. The  $^{13}\text{C}$  recoil polar angle  $\theta$  is plotted vs. the ion momentum.

Another motivation for the recoil method is kinematical in nature: in the laboratory, the heavy particle is emitted in a limited range of angles with respect to the beam direction. Fig. 2.7 describes the kinematics of  $^{12}\text{C}(p, \pi^+)^{13}\text{C}_{\text{g.s.}}$  for proton beam energies in the range covered by the CE-06 experiment. Close to threshold ( $E_p < 170$  MeV), the  $^{13}\text{C}$

recoils are emitted in a narrow forward cone with  $\theta_{\max} \lesssim 7^\circ$ . Even 200 MeV above the reaction threshold, the maximum recoil emission angle is less than  $20^\circ$  with respect to the incident beam direction. This kinematical “compression” from the center-of-mass system to the laboratory frame allows solid angles which are reasonably achieved in the lab (e.g.,  $\Omega \approx 10$  msr) to correspond to nearly  $4\pi$  acceptance in the c.m.s., near threshold. Other authors ([Sc86], [Ho87]) have demonstrated the feasibility of studies of near-threshold  $\pi^+$  production in light nuclei, using recoil detection techniques.

A third reason to use the recoil method is the ability to measure neutral-pion reactions along with the corresponding charged-pion states via the same experimental apparatus. By detection of the recoil, the difficulties involved in the coincident measurement of high-energy  $\gamma$  rays (from  $\pi^0 \rightarrow \gamma\gamma$ ) are avoided. With the exception of a single, very near-threshold measurement [Pi93], the only reported  $A(p, \pi^0)A+1$  work (with  $A > 4$ ) has used the recoil method [Ho92] (the data from which is shown in Fig. 2.6).

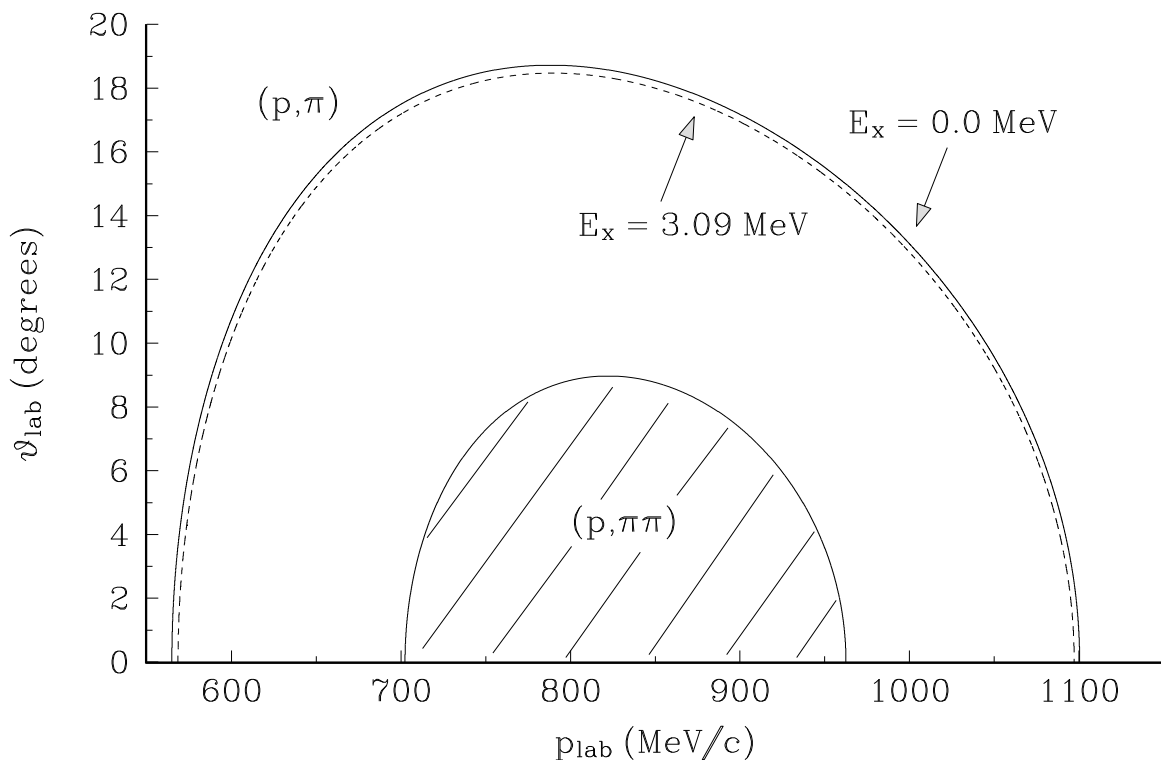


*Figure 2.8* The recoil ion kinematics ( $E_p = 330$  MeV) of  $^{12}\text{C}(p, \pi^+)^{13}\text{C}$  (two-body final state) compared to  $^{12}\text{C}(p, \pi^+\pi^0)^{13}\text{C}$  (three-body final state). The locus of single-pion events lies only along the curves shown ( $^{13}\text{C}$  ground state and first excited state), and so is well-separated from the two-pion locus.

Finally, the recoil method can greatly simplify the measurements of reactions which

lead to three-body final states, such as  $^{12}\text{C}(\text{p}, \pi\pi)$ . Although two-pion final states with the same charge as corresponding single-pion emissions lead to identical types of recoil ions, the single- and double-pion production kinematics are well-separated, as shown in Fig. 2.8. The complete identification of an  $M = 13$  nucleus within the shaded area of the figure corresponds uniquely to a double-pion production reaction.

The remainder of this work details the study of proton-induced, single- and double-pion production from  $^{12}\text{C}$  as realized in the CE-06 experiment, which was developed and carried out at the Indiana University Cyclotron Facility in 1991–93. Since much near-threshold  $^{12}\text{C}(\text{p}, \pi^+)^{13}\text{C}$  work has already been done, the primary goals of CE-06 are to study the  $^{12}\text{C}(\text{p}, \pi^0)^{13}\text{N}$  reaction (addressing in particular the anomaly of Fig. 2.6) and to attempt the first measurements of double-pion production in light nuclei near threshold.